Mansoura Journal of Chemistry Vol. 38 (2), December, 2011.

SYNTHESIS AND PHYSICOCHEMICAL PROPERTIES OF ZR-MCM-41CATALYST

S.E. Samra*, H. A. Moustafa, A.S. Khder, A. M. Ouf and A. A. Ibrahim
Chemistry Department, Faculty of science, Mansoura University,
35516- Mansoura, Egypt

(Received: 20 / 11 / 2011)

ABSTRACT

Zr-containing MCM-41 catalysts were prepared by hydrothermal method. The obtained samples were characterized by XRD, FTIR and N_2 physical adsorption. The surface acidity was measured by potentiometric titration and FTIR spectra of chemically adsorbed pyridine. The results show that the samples possess typical hexagonal mesoporous structure of MCM-41 and high specific surface areas. The characterization results showed that Zr was highly dispersed in the tetrahedral environment of silica framework. The ordering of Zr-MCM-41 was also influenced by the content of Zr, which decreased gradually with the increase of Zr content. The acidity measurements showed that the total acidity increases with the rise of Zr content up to 15wt%. FTIR spectra of pyridine adsorbed on the catalysts showed the presence of both Brønsted and Lewis acid sites. An optimum reaction performance (24.2% of 7-hydroxy-4-methyl coumarin formed) was achieved at 15 wt% loading of Zr.

Key words:- Synthesis , Physicochemical properties , ZR-MCM-Catalyst

INTRODUCTION

Since the discovery of ordered mesostructured materials **[Kresge *et al.*, (1992)]**, there have been continuous efforts to utilize MCM-41 and related molecular sieves as catalysts **[Thomas, (1994)]**. The large pore sizes compared to microporous zeolites provide an unlimited diffusion of reactants through the pores, which enable the reactions involving bulky molecules to take place. The ordered mesoporous materials due to their pore diameters can overcome the disadvantage of zeolites **[Xu *et al.*, (2007)]**, since they can host metallic and acid catalytic sites within a larger volume where the transformation of much larger molecules is possible. In general, the structural and textural characteristics of such molecular sieves are directly related to the synthesis conditions: the type of surfactant, pH, and presence of electrolytes, temperature, solvents and ageing/preparation time **[Occelli *et al.*, (2000) ; Lindlar *et al.*, (2001) ;**

Occelli *et al.*,(2003) and Selvam *et al.*, (2000)]. These characteristics of MCM-41 enables itself a potential candidate for inclusion of guest species inside its mesopoures.

Recently, many efforts have been made by worldwide researchers for the modification of the pure silica MCM-41 mesoporous molecular sieve in order to enhance its practicability. Of which the incorporation of transition metal ions into the pure silica MCM-41 framework for promoting the thermal and hydrothermal stabilities and surface acidity has been found to be an effective strategy. Consequently, the study of metal based mesoporous composites has been a hot subject. The incorporation of heteroatoms into mesoporous silica framework has been widely investigated. Various

transition metal ions such as Ti **[Selvaraj *et al.*, (2005)]**, V **[Gucbilmeza *et al.*, (2005)]**, Fe, Nd, **[Lim *et al.*, (2005)]**, Co **[Igarashi *et al.*, (2005)]**, Ce **[Lin *et al.*, (2009)]**, Zr **[Kong *et al.*, (2005)]**, Ni **[Occelli *et al.*, (1999)]** and Al **[Gontier & Tuel (1996)]** have been incorporated into the framework of MCM-41 in order to improve its acid and/or redox properties. Zirconium is a special transition metal oxide that possesses not only weak acid and base properties but also redox activities. Moreover, the mixed oxides generate some particular properties, which are not possessed by the silica or transition metal oxide alone. For example, it has been reported that zirconium incorporated mesoporous silica exhibited strong acidity, although the acidities of both zirconia and silica are weak **[Bianchi *et al.*, (2001) ; Shibata *et al.*, (1973) and Salasa *et al.*, (2009)]**. However, its relatively low surface area (usually below 50 m^2 g^{-1}) limits the number of active sites **[Yamaguchi (1994)]**. In the last few years, zirconium containing mesoporous materials have been paid much attention because of their potential applications in heterocatalysis, petroleum processing, etc. Many efforts have been made by incorporating zirconium ions into the siliceous framework of MCM-41 mesoporous molecular sieve **[Chen *et al.*, (2006) and Infantes *et al.*, (2004)]**. However, most of the previous reports focused on the hydrothermal synthesis of Zr_containing mesoporous molecular sieve and the investigation of the catalytic property. Comparison of synthesis of Zr-MCM-41 mesoporous molecular sieve through different methods and the study on the thermal and hydrothermal stabilities was seldom systematically reported.

The aim of this study is to investigate the modifications of the framework of MCM-41 by incorporation in situ of Zr ions in order to obtain a supported Zr–MCM-41 catalyst. A detailed characterization of the materials was made using X-ray diffraction (XRD), The FT-IR spectra, N_2 adsorption–desorption isotherms.

EXPERIMENTAL

Catalyst Preparation

MCM-41 materials were prepared as **[Terres & Dominguez (2003)]** reported. Cetyltrimethyl ammonium bromide (CTAB) ($C_{19}H_{42}NBr$) was tenso-active materials which together with ammonium hydroxide (NH_4OH) were added to deionized water at room temperature. Both were previously weighted according to the molar ratio (CTAB/ TEOS = 4.08 and CTAB/NH_4OH = 0.21) used for the synthesis; the mixture was stirred during 45 min, later tetraethyl orthosilicate (TEOS) ($C_8H_{20}O_4Si$) was added to the mixture as a source of silica. The product was filtered, washed with distilled water and

dried in air at 120°C. The template was removed by calcination in synthetic air at 550°C for 10 hr using a heating rate of 5°C/min.

The mesoporous support was impregnated with an aqueous solution of zirconium oxy chloride of 2, 8, 15, 25, 50 and 75 wet%. After impregnation, the catalysts were dried at 120°C overnight in air and calcined in synthetic air at 550°C for 3 hr. The catalysts are denoted as XZr-MCM-41 (X being the loading, in wt %).

Catalyst Characterization

XRD Investigation

The powder diffraction patterns were recorded on X- ray powder diffractometer (XRD) PW 150 (Philips) using Ni filtered Cu Kα radiation (λ= 1.540Å) at 40 kV, 30 mA and a scanning range 2θ of 1 to 70°. The distance from center to center in pores was calculated from Bragg law using the position of the first X-ray diffraction line (d_{100}). The reticular parameter a_0 of the hexagonal cell unit was calculated by $a_0 = 2d_{100}/\sqrt{3}$ equation **[Matsuhashi *et al.*, (1994)].**

Surface Area Measurement

Surface area and pore properties of samples were analyzed using the high vacuum conventional volumetric glass system. Prior to any adsorption measurement the sample was degassed at 250°C for 4hrs under a reduced pressure of 10^{-5} Torr following the BET procedure using N_2 as adsorbent at liquid nitrogen temperature. The surface area was calculated from adsorption isotherms by the BET method, and the pore size distribution in the mesopores region was determined by applying the BJH method to the desorption branch of the isotherm. The total pore volume (Vp) was determined by nitrogen adsorption at a relative pressure of 0.98 and the mesopore diameter (dp) corresponded to the maximum of the pore size distribution. Pore wall thickness was assessed by subtracting dp from the a_0 unit-cell parameter which corresponded to the distance between the centers of adjacent mesopores.

Surface Acidity Measurements.

Pyridine adsorption

Lewis and Bronsted acid sites presented on the surface were determined with FT-IR spectra of adsorbed pyridine. Prior to the pyridine adsorption **[Beck *et al.*, (1992)]**. the samples were degassed at 200°C for 3 hrs under high vacuum followed by soaking suspending in a dried pyridine. Then, the excess pyridine was removed by evaporation. The FT-IR spectra of the samples were conducted using MATTSON 5000 FTIR spectrophotometer; by mixing 0.005 g of the sample with 0.1 g KBr in 30 mm diameter self supporting discs were used.

Catalytic activity

The Synthesis of 7-hydroxy-4-methyl coumarin was carried out by using resorcinol (10 mmol) and ethylacetoacetate (20 mmol) with 0.1g of the activated catalyst (at 120°C for 2 hrs). The reaction was carried out in oil bath at 120°C under stirring and reflux for 2 hrs. After the reaction, the product was separated by transferring the hot reaction mixture in ice bath and stirring for about 15 min, then filtration. The % yield of 7-hydroxy-4-methyl coumarin was calculated as follows:

$$\text{Yield (wt\%)} = \left(\frac{\text{Obtained weight of product}}{\text{Theoretical weight of product}}\right) \times 100$$

RESULTS AND DISCUSSION

X-ray diffraction

The XRD patterns of pure siliceous MCM-41 and Zr-MCM-41 with Zr wet% of 2.0, 8.0, 15 and 50 are displayed in **Fig. (1)** . All samples have a diffraction peak at 2θ value of 2.21, which corresponded to (100) reflection of the mesoporous material **[Beck *et al.*, (1992)]**, indicating that the Zr-MCM-41 samples possess the mesoporous framework. Furthermore, with the increase in zirconium content, the diffraction peak (100) of the Zr-MCM-41samples gradually weakened and broadened, and the main peak intensity decreased, suggesting that the mesoporous ordering gradually deteriorated with the increase in zirconium content. This probably owes to an increasing number of defect sites and bond strain in these materials **[Velu *et al.*, (2002)]**. As shown in **Fig. (1a)**, other(110) and (200) reflections of high order for MCM-41 sample appear at 2θ = 3.7 and 4.4, respectively, indicating that the channels are hexagonally organized and the ordered MCM-41 structure is formed because the typical Bragg reflections of hexagonal MCM-41 mesoporous material appear at low angles **[Matsuhashi *et al.*, (1994)]**. However, from **Fig. (1B, C, D)** and it can be observed that, by increasing Zr content the Zr-MCM-41 samples have weak diffraction peaks at (110) and (200). This indicates that a gradual loss of long-range ordering occurs with increasing in corporation of Zr in the Zr-MCM-41 samples. The peak intensity of (1 0 0) planes gradually decreased and the diffraction peaks of (1 1 0) and (2 0 0) planes gradually disappeared with the increase of Zr content, which meant that the ordering of Zr-MCM-41 samples decreased when more and more Zr was incorporated into the framework of MCM-41. It was probably that the different ionic radius of Zr (0.84 A°) and Si (0.41 A°) made Zr in the deformed-tetrahedral coordination inside the framework, and thus the high Zr content resulted in the low ordering of the structure. Concomitantly, the decrease in the structural ordering rendered the decrease of the surface area **Table (1)** when the Zr content increased. A similar situation has been observed in MCM-41containing other metals **[Zhan *et al.*, (2008)]**. Loss of crystallinity is observed for Zr-impregnated samples as the intensities of the higher angle peaks diminished **Fig. (1b)** . This indicates that Zr may have rather homogeneously dispersed onto the interior surface of MCM-41. The hexagonal unit cell parameter a_0 was calculated from the equation $a_0 = 2d_{100}/\sqrt{3}$, which was obtained from the peak in the XRD pattern by Bragg's equation ($2d\sin\theta = \lambda$, where λ = 1.5406 A ° for the Cu Ka radiation line). The value of a_0 was equal to the internal pore diameter plus pore wall thickness. Physicochemical properties of these mesoporous materials were summarized in **Table (1)**. The d_{100} values are given in **table (1)** along with corresponding unit cell parameters (a_0). No apparent changes in unit cell parameters are observed in the case of Zr-MCM-41. It may be inferred that most of the Zr are not incorporated into the framework position of MCM-41.

Table (1): Physicochemical properties of different Zr-MCM-41 samples

Samples	D_{100} (nm)	a_o (nm)	S_{BET} m^2/g	d_B BJH (nm)
MCM-41	35.9	41.5	1007.6	22.1
2ZM	36.7	42.4	935.2	23.3
8ZM	35.9	41.5	875.2	22.5
15ZM	35.9	41.6	726.2	21.2
50ZM	35.2	40.6	585.8	22.5

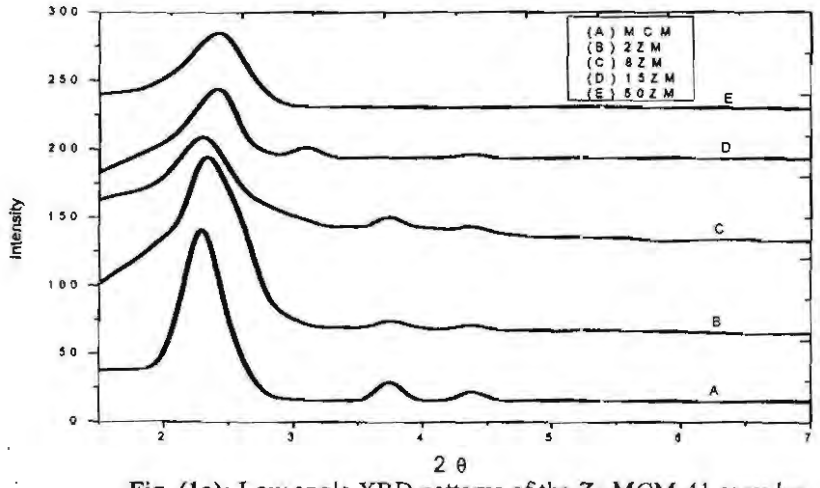

Fig. (1a): Low angle XRD patterns of the Zr-MCM-41 samples

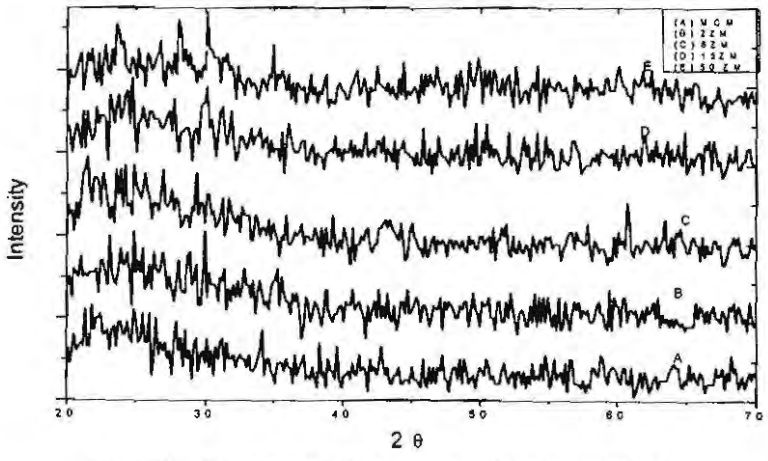

Fig. (1b): High angle XRD patterns of the Zr-MCM-41.

Framework IR spectroscopy

The FT-IR spectra of **Fig. (2)** were recorded in the 400-4000 cm–1 range, and it demonstrated the framework vibration of Zr-MCM-41 materials **Fig. (2B, C)** which was similar to that of the MCM-41 material **Fig. (2A)**. The broad bands around 3450 cm^{-1} may be associated with surface silanols and adsorbed water molecules, while deformational vibrations of adsorbed molecules caused the absorption bands at 1637 cm^{-1} **[Rana & Viswanathan (1998)]**. The intensity of 1637 cm^{-1} band did not change significantly with the variety of Zr-containing MCM-41, indicating a residual concentration of OH groups on all the samples due to the fact that isomorphous substitution occurred inside pore wall for MCM-41. All the samples exhibit also two more bands at 795 and 456 cm^{-1} are ascribed to symmetric stretching vibration and bending vibration of rocking mode of Si–O– Si, respectively. All the samples exhibit also the anti-symmetric vibration band at 1080 cm^{-1}, which is characteristic for the tetrahedral SiO_4^{4-} structural units. Furthermore, a strong band at around 952 cm^{-1} was clearly visible in the FT-IR spectra of MCM-41, which could be contributed to the stretching vibration of Si–O-groups vibration in molecular sieves **[Notari (1989)]**, the information of Zr–O–Si linkages and oxygen-deficient centers The Si–OH rocking peak at 952 cm–1 disappeared, suggesting interaction between the surface silanol groups with neighboring Zr cations

The vacancy will be filled by the incorporation Zr, resulting in the decrease of intensities of the band. However, a band at 952 cm^{-1} is also observed in the Al-MCM-41 sample without any shift, and is assigned to (Si-O-Al) in the calcined state **[Dawn et al., (1996)]**. Therefore, because the intensity of this band shows no change with changing Zr content, it cannot be taken as a proof for Zr incorporation into the framework of Zr-MCM-41.

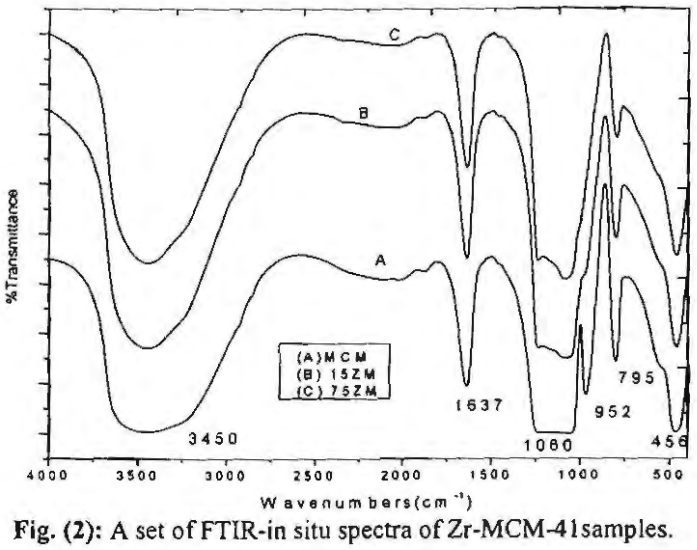

Fig. (2): A set of FTIR-in situ spectra of Zr-MCM-41samples.

Adsorption isotherm of nitrogen

In order to evaluate the porosity of the materials, N_2 adsorption was carried out. **Figure (3)** shows the N_2-adsorption–desorption isotherm for Zr-MCM-41 with pore-size distribution curve. For all samples, the isotherms are similar having inflection around $P=P0$ = 0.20–0.30 characteristic of mesoporous materials with uniform pore size **[Beck *et al.*, (1992)]**. Surface area calculated by BJH method, average pore sizes and specific pore volume for the various samples are given in **table (1)**. The decrease in surface area for the impregnated samples can be attributed to the loss in crystallinity seen in the XRD patterns. There was no appreciable variation in the pore sizes among Zr-MCM-41 and siliceous MCM-41 samples. Wall thickness calculated by subtracting pore diameter from a_0 unit cell parameter shows there is constancy in thickness for Zr-containing samples from that of pure siliceous MCM-41 indicating thus a uniform distribution of Zr around the pore mouth. This constancy in wall thickness for Zr-MCM-41 is in the same range as reported by Zhang et al. **[Zhang et al., (1996)]** for Ti-MCM-41, where they have attributed this to the metal uniform distribution around the pore mouth of the mesoporous silicate framework. Decrease in pore size and pore volume for the impregnated samples shows that the pore surface is covered by zirconium species, which is further evident from the increase in wall thickness. The specific surface area of samples from

The BET method ranges between 1007.2 and 585 m^2/g **Table (1)**. The narrow pore size distribution of the Zr-MCM-41 implies that the zirconium ions are homogeneously distributed across the MCM-41 and pore blockage did not take place **Fig. (4)** and **Table(1)**. The pore size distributions see **Fig. (4)** revealed sharp peaks for all samples, meaning that all samples possessed uniform pore sizes. Furthermore, the BET surface area, the pore diameter, pore volume and wall thickness were summarized in **Table (1)**. With respect to **Table (1)**, the appropriate incorporation of Zr could favor the formation of better organized mesoporous materials due to radius effect of Zr atoms using TEOS as silica source in preparation process. Superfluous introduction of Zr ions conducted to the less well-ordered hexagonal arrangement and formation of ZrO_2 nanoclusters. Radius of Si^{4+} (40 pm for 4-coordinate, tetrahedral) was less than that of Zr^{4+} (73 pm for 4-coordinate, tetrahedral and 86 pm for 6-coordinate, octahedral). From **Table (1)**, we can conclude that the specific surface area and pore volume of the resulting samples gradually decreased as the zirconium content increased, and that the pore size is in the range of 2.5–2.9 nm. Combined with the results of XRD and N_2 adsorption isotherms, it is reasonable to conclude that Zr could favor the formation of better organized mesoporous.

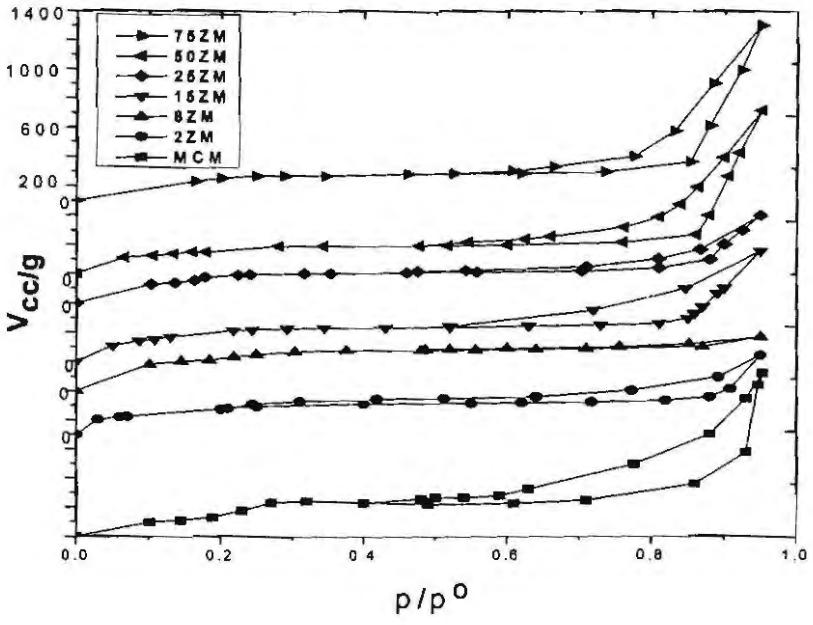

Fig. (3): A set of N2 adsorption–desorption isotherm of Zr-MCM-41samples.

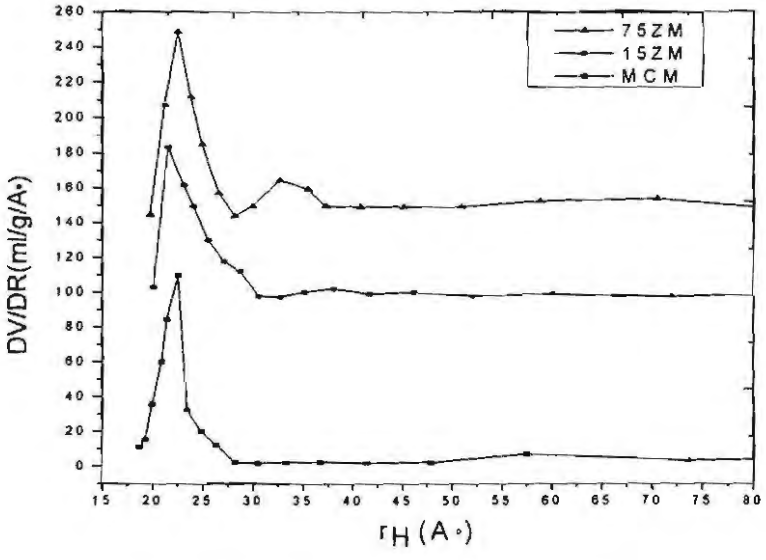

Fig. (4): A set of Pore diameter distribution curves of Zr-MCM-41samples.

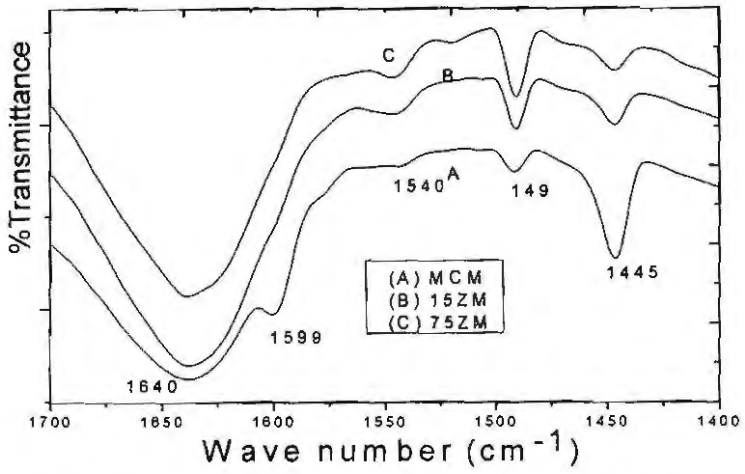

Fig. (5): A set of in situ FT-IR spectra of pyridine adsorption on the Zr-modified MCM-41 samples.

Surface Acidity

The surface acidity of the samples was determined by the in situ FT-IR of pyridine adsorption technique. **Fig. (5)** shows a set of in situ-FT-IR spectra of pyridine adsorption on the samples of Zr-MCM-41. Lewis acid sites existed on the surface as characterized by the formation of the bands at 1445, and 1599 cm^{-1} **[Devassy *et al.*, (2005)]**. In addition, a band corresponding to vibration of pyridine associated with both, Lewis and Bronsted acid sites, was observed at 1490 cm^{-1} (noted as B+ L acid sites) **[Jermy & Pandurangan (2005)]**. An absorption band at 1540 cm^{-1} appeared, showing that Bronsted acid sites were formed in the sample. The band at 1640 cm^{-1} was assigned to pyridine adsorbed on the hydroxyls ions.

On the MCM-41 sample, the bands corresponding to pyridine adsorbed on Lewis acid sites at 1450 and 1590 cm^{-1} were observed **Fig. (5)**. However, there was a weak band at 1540 cm^{-1} appeared, indicating the formation of a small number of Bronsted acid sites in this sample. These results indicate that the interaction between pyridine and the MCM-41 sample is very weak and thus the acid strength. In comparison with the MCM-41 sample, the intensities of the bands corresponding to both Bronsted acid sites and Lewis + Bronsted acid sites, of the Zr modified sample are increased.. These results show that the addition of zirconium not only creates Bronsted acid sites but also decrease strength of Lewis acid sites. It is well known that the Zr^{4+} diameter is much larger than that of Si^{4+} ions; when the smaller Si^{4+} ions were replaced by the larger Zr^{4+} ion in the framework of the solid, the bond length of Zr-O- Si clearly differs from the one of Si-O-Si, this must lead to some structure deformation, microstrain is generated in the lattice cell accordingly. As shown in **Figs. (1 and 2)**, many silanol groups exist in the structure of the solids and the presence of small amounts of zirconia may affect the strength of the SiO-H bonds. Changes in the electron density around Si, due to charge unbalance, or differences in electronegativity or local structure deformation resulting from the introduction of the Zr^{4+} ion into the vicinity of the hydroxyls carrying silicon, may weaken the SiO-H bond **[Hoefnagel *et al.*, (1995)]**, this is one of the possible

origins giving rise to the generation of Bronsted acid sites on the Zr-MCM-41 solid. zirconium is considered to be important because of the possible strong polarization of the $Si–O^{-\delta}\cdots Zr+^{\delta}$ linkages **[Eswaramoorthi *et al.*, (2004)].**

Catalytic activity

Examination of **Fig. (6)** and **table (1)** shows that the formation of 7-hydroxy-4-methylcoumarin increases gradually with increasing the amount of Zr loaded on MCM-41 till reaches the maximum (21.2%) at 15-Zr-MCM-41. From **Fig. (6)** it was found that the catalytic activity, Brönsted and Lewis sites increased with increased Zr loading up to 15 wt% but then decreased with further increases in Zr content. Thus the sample 15-Zr-MCM-41 had the highest acidity. The ratio of resorcinol: EAA, 1:2, was found to be optimum for the solvent free synthesis of coumarin. Similar results were reported by **[Marosi *et al.*, (2000)]** and **[Palaniappan *et al.*, (2004)].** The observed decrease in the catalytic activity with further increase in the ethylacetoacetate molar ratio can be explained by the saturation of the catalyst surface with the ethylacetoacetate; thereby blocking the acid adsorption centers. Thus, we can say there is a competitive adsorption of the ethylacetoacetate on the acid sites with resorcinol, which reduces the efficiency of the catalyst **[Hill & Posser (1995)].** Several studies have been carried out to study the effect of solid acid catalysts on coumarin synthesis, however, with different observations **[Wang et al., (2003) and Hoefnagel *et al.*, (1995)].**

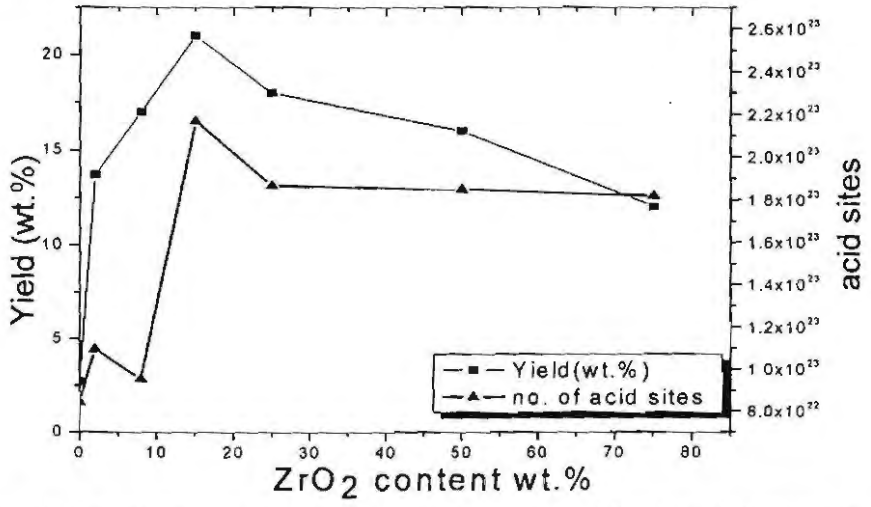

Fig. (6): The relationship between Zr content, Brönsted and Lewis acid sites for the formation of 7-hydroxy-4-methylcoumarin.

CONCLUSIONS

Zr-MCM-41 catalyst has been prepared by hydrothermal method. Prepared catalyst has high acidity and contain both bronsted and lewis acid site. It was found that the maximum yeiled of 7-hydroxy-4- methylecoumarin achieved at 15%Zr-MCM-41

REFRENCE

Beck J.S., Vartuli J.C., Roth W.J., Leonowicz M.E., Kresge C.T., Schmitt K.D., Chu .T.W., Olson D.H., Sheppard E.W., J.Am.Chem. Soc. 114, 10834 (1992).

Bianchi A.O., Campanati M., Maireles T. P., Rodriguez C E., Jimenéz L. A., Vaccari A., Appl. Catal. A 220, 105 (2001).

Chen L.F., Nore˜a L.E., Navarrete J., and Wang, J.A., Mater. Chem.Phys. 97, 23 (2006).

Cielsa U., Schuth F., Microp. Mesop. Mater. 27, 149 (1999)

Dawn A. M., Luan Z., Klinowski J. J., Phys Chem 100, 2178 (1996)

Devassy B.M., Lefebvre F., Halligud S.B., J. Catal., 231, 1 (2005).

Eswaramoorthi I., Sundaramurthy V., Lingappan N., Microp. Mesop. Mater, 71, 109 (2004).

Gontier S., Tuel A., Appl. Catal. A 143, 125 (1996).

Gucbilmeza Y., Dogua T., Balci S., Catal. Today 100, 473 (2005).

Hill C.L., Posser C.M., Coord. Chem. Rev. 143, 407 (1995).

Hoefnagel A.J., Gunnewegh E.A., Downing R.S., van Bekkum H., J. Chem. Soc.Chem. Commun. 225, 171 (1995).

Igarashi N., Kidani S., Ahemaito R., Hashimoto K., Tatsumi T., Micropor. Mesopor. Mater., 81, 97 (2005).

Infantes M. A., Me_rida_Obles J., Maireles T. P., Micropor.Mesopor. Mater. 75, 23 (2004)

Jermy B.R., Pandurangan A., J. Mol. Catal. A: 237, 146 (2005).

Kong Y., Guo X., Zhang F., Jiang S., Wang J., Lu Y., Yan Q., Mater. Lett. 59, 3099 (2005).

Kresge C.T., Leonowicz M.E., Roth W.J., Vartuli J.C., and Beck J.S., Nature 359, 710 (1992).

Lim S., Yang Y., Ciuparu D., Wang C., Chen Y., Pfefferle L., Haller G.L., Top. Catal. 34, 31 (2005).

Lin K., Pescarmona P.P., Houthoofd K., Liang D., Tendeloo G.V., Jacobs P.A., J. Catal. 263, 75 (2009).

Lindlar B., Kogelbauer A., Kooyman P.J., Prins R., Micropor. Mesopor. Mater., 89, 44 (2001)

Marosi L., Cox G., Teten A., Hibst H., J. Catal. 194, 140 (2000).

Matsuhashi H., Motoi H., Arata K., Catal. Lett. 26, 325 (1994).

Notari B., Stud. Surf. Sci. Catal. 37, 413 (1989)

Occelli M.L., Biz S., Auroux A., Appl. Catal. A 183, 231 (1999).

Occelli M.L., Biz S.J., Catal Rev Sci Eng 40, 329 (2003)

Occelli M.L., Biz S.J., J Mol Catal A 151, 225 (2000)

Palaniappan S., Shekhar R.C., J. Mol. Catal. A: Chem. 209, 117 (2004).

Rana R.K., Viswanathan B., Catal Lett 52, 25 (1998).

Salasa P., Wang J.A., Armendariz H., Angeles C. C., Chen L.F., Mater.Chem. Phys. 114, 139 (2009).

Selvam P., Badamali S., Sakthivel A., Catal Today 63, 291 (2000)

Selvaraj M., Sinha P.K., Lee K., Ahn I., Pandurangan A., Le T.G., Micropor. Mesopor. Mater. 78, 139(2005).

Shibata K., Kiyoura T., Kitagawa J., Sumiyoshi T., Tanabe K., Bull. Chem. Soc. Jpn. 10, 2985 (1973).

Terres E., Dominguez J.M, Microp. Mesop. Mater. 66, 348 (2003)

Thomas J.M., Nature 368 289 (1994).

Velu S., Wang L., Okazaki M., Suzuki K., Tomura S., Microp. Mesop. Mater. 54, 113 (2002).

Wang L., Xia J., Tian H., Qian C., Ma Y., Int. J. Chem. 42B, 2097 (2003).

Xu R., Pang W., Yu J., Huo Q., Chen J., Chemistry of Zeolites and Related Porous Materials: Synthesis and Structure, Wiley & Sons (Asia), Singapore, 2007.

Yamaguchi T., Catal. Today 20, 199 (1994).

Zhan W.C., Lu G.Z., Guo Y.L., Guo Y., Wang Y.S., J. Rare Earths 26, 59 (2008).

Zhang W., Froba M., Wang J., Tanev P.T., Wong J. and Pinnavaia T.J., Am J.Chem. Soc. 118, 9164 (1996).

الملخص العربي

تحضير ودراسة الخواص الفيزوكيميائية لحفاز الزركونيوم المحملة علي السليكا المطورة

سالم السيد سمره* - هاتم عبدالرسول مصطفي – عبدالرحمن صلاح خضر - عبدالفتاح محمد عوف
قسم الكيمياء – كلية العلوم – جامعة المنصورة – ٣٥٥١٦- المنصورة – جمهورية مصر العربية

تم تحضير حفازات الزركونيوم المحملة علي السليكا المطورة بطريقة تأثير حرارة الماء كما تم توصيفها باستخدام تقنية حيود الاشعة السينية و امتزاز غاز النيتروجين السائل علي سطح الحفازات. درست الخواص الحمضية للحفازات المحضرة عن طريق المعيارة مع ن- بيوتيل امين وكذلك امتزاز غاز البيريدين علي سطح الحفاز.وقد اظهرت النتائج ان العينات تتميز بمساحة سطح عالية بالاضافة الي وجود شكل سداسي للمسامات. ووجد توزيع جيد للزركونيوم علي سطح السليكا المطورة ولكن تأثر ترتيب السطح بزيادة نسبة تحميل الزركونيوم علي سطح السليكا المطورة. واظهرت القياسات لحامضية زيادة حامضية السطح حتي ١٥ % تحميل الزركونيم ووجد ان هذه النسبة تعطي اعلي معدل لانتاج مشتقات الكومبرين.